



HAL
open science

Interfacial Dynamics and Rheology of a Crude-Oil Droplet Oscillating in Water at a High Frequency

Nicolas Abi Chebel, Antoine Rémy Piedfert, Benjamin Lalanne, Christine Dalmazzone, Christine Noïk, Olivier Masbernat, Frédéric Risso

► **To cite this version:**

Nicolas Abi Chebel, Antoine Rémy Piedfert, Benjamin Lalanne, Christine Dalmazzone, Christine Noïk, et al.. Interfacial Dynamics and Rheology of a Crude-Oil Droplet Oscillating in Water at a High Frequency. *Langmuir*, 2019, 35 (29), pp.9441-9455. 10.1021/acs.langmuir.9b01594 . hal-02294205

HAL Id: hal-02294205

<https://hal.science/hal-02294205v1>

Submitted on 23 Sep 2019

HAL is a multi-disciplinary open access archive for the deposit and dissemination of scientific research documents, whether they are published or not. The documents may come from teaching and research institutions in France or abroad, or from public or private research centers.

L'archive ouverte pluridisciplinaire **HAL**, est destinée au dépôt et à la diffusion de documents scientifiques de niveau recherche, publiés ou non, émanant des établissements d'enseignement et de recherche français ou étrangers, des laboratoires publics ou privés.








Open Archive Toulouse Archive Ouverte (OATAO)

OATAO is an open access repository that collects the work of Toulouse researchers and makes it freely available over the web where possible

This is an author's version published in: <http://oatao.univ-toulouse.fr/24245>

Official URL: <https://doi.org/10.1021/acs.langmuir.9b01594>

To cite this version:

Abi Chebel, Nicolas  and Piedfert, Antoine Rémy  and Lalanne, Benjamin 
and Dalmazzone, Christine and Noik, Christine and Masbernat, Olivier  and
Risso, Frédéric  *Interfacial Dynamics and Rheology of a Crude-Oil Droplet
Oscillating in Water at a High Frequency*. (2019) *Langmuir*, 35 (29). 9441-9455.
ISSN 0743-7463

Any correspondence concerning this service should be sent
to the repository administrator: tech-oatao@listes-diff.inp-toulouse.fr

Interfacial Dynamics and Rheology of a Crude-Oil Droplet Oscillating in Water at a High Frequency

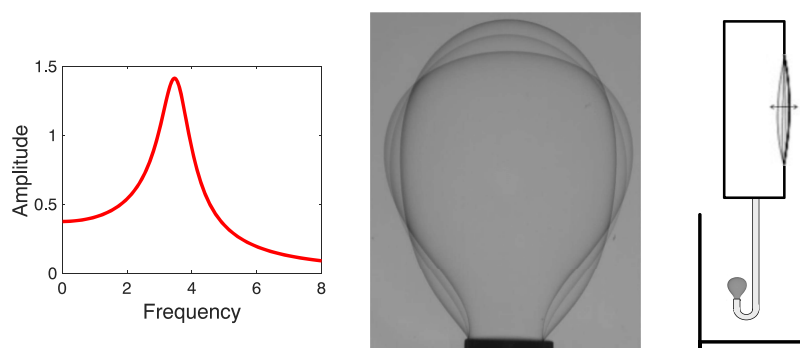
Nicolas Abi Chebel,^{†,‡,||} Antoine Piedfert,^{†,‡,||} Benjamin Lalanne,^{‡,||} Christine Dalmazzone,^{§,Ⓜ} Christine Noïk,^{§,Ⓜ} Olivier Masbernat,^{‡,||} and Frédéric Risso^{*,†,||,Ⓜ}

[†]Institut de Mécanique des Fluides de Toulouse (IMFT), Université de Toulouse, CNRS, 31400 Toulouse, France

[‡]Laboratoire de Génie Chimique (LGC), Université de Toulouse, CNRS, 31432 Toulouse, France

[§]IFP Energies nouvelles, 1-4 avenue de Bois Préau, 92852 Reuil-Malmaison, France

^{||}FR FERMAT, Université de Toulouse, CNRS, INPT, INSA, UPS, Toulouse, France



ABSTRACT: We report investigations of a pendant diluted crude-oil droplet in water that is forced to oscillate at a frequency ω . The droplet interface contains a significant amount of surface-active agents and displays a marked viscoelastic rheology with elastic moduli larger than viscous ones. At a low frequency, fluid viscosity and inertia are negligible, which allows a direct determination of the dilatational interface rheology. At a large frequency, eigenmodes of inertial shape oscillations are excited. By decomposing the interface shape into spherical harmonics, the resonance curves of the inertial modes of the interface are determined, as well as the frequency and damping rate of each mode. These two parameters are of major importance for the prediction of the deformation and breakup of a droplet in any unsteady flow without any prior knowledge of either the chemical composition or the detailed rheological properties of the interface. Then, interfacial rheology is related to interface dynamics by solving the coupled dynamic equations for the two fluids and the interface. It turns out that the rheology of the interface is well described by an equivalent two-dimensional viscoelastic material, the elasticities and viscosities of which depend upon the frequency. A first significant result is that shear and dilatational elasticities are closely connected, as are shear and dilatational viscosities. This implies that intrinsic rheology plays a major role and that compositional rheology is either negligible or strongly coupled to the intrinsic one. A second major result is that, for moderately aged droplets (≤ 5000 s), the elasticity and viscosity at a high frequency (10–80 Hz) can be extrapolated from low-frequency measurements (≤ 1 Hz) by a simple power law of the frequency, ω^z . The exponent z is related to the loss angle θ_{loss} by a relation found in many previous low-frequency investigations of crude-oil interfaces: $z = \theta_{\text{loss}}/2\pi$. The present work thus extends classic observations obtained at a low frequency to a higher frequency range corresponding to the natural frequency of the droplets, where the droplet shape results from the balance between dynamic pressure and surface stresses and the interface involves simultaneous shear and dilatation. These results bring about serious constraints regarding the modeling of physicochemical underlying mechanisms and provide some insights for the understanding of the structure of crude-oil interfaces.

■ INTRODUCTION

The original motivation of this work is to predict how a crude oil–water interface deforms and eventually ruptures, which is of special importance for the prediction of droplet size distributions and the stability of petroleum emulsions.

The deformation of a droplet results from the response of the interface to the hydrodynamic stress exerted by the surrounding fluid.¹ Provided the fluids are not too viscous, the interface dynamics is characterized by a series of eigenmodes of

oscillations.² (Low viscosity means that the Ohnesorge number should be small: $Oh = \frac{\eta_i}{\sqrt{\rho_i d \gamma}} \ll 1$, where ρ_i and η_i are respectively the density and the viscosity of the inner fluid, d is the droplet diameter, and γ is the interfacial tension). Each of

these modes, defined by its order $n \geq 2$, is characterized by a specific shape, an angular frequency ω_n , and a damping rate β_n .³ A droplet that is initially deformed according to mode n and released in a fluid at rest performs damped oscillations at frequency ω_n with an amplitude that exponentially decays with time at a rate β_n , until it eventually reaches a spherical shape. These oscillations result from the periodic exchange between the kinetic energy of the fluids and the potential energy stored in the deformed interface. Both ω_n and β_n are increasing functions of n and decreasing functions of the droplet size, whereas the ratio β_n/ω_n is a decreasing function of d . In many situations involving droplet emulsions, the frequencies are large and the damping rates are small compared to the frequencies. Let us consider a droplet of heptane in water: for $d = 0.1$ mm, $Oh = 7 \times 10^{-3}$, $\omega_2/2\pi \approx 7 \times 10^3$ Hz, $\beta_2 \approx 4 \times 10^3$ s⁻¹; for $d = 5$ mm, $Oh = 10^{-3}$, $\omega_2/2\pi \approx 20$ Hz, $\beta_2 \approx 4$ s⁻¹. Because they are easier to excite, the lower-order modes are most often sufficient to describe the main deformation of a droplet. In particular, it has been shown that the breakup of a droplet in a turbulent flow essentially depends on ω_2 and β_2 and on the properties of turbulence.^{4–6} It is important to stress that these modes involve frequencies of at least several tens of hertz, which implies that the knowledge of the response of the interface at such large frequencies is of primary importance.

In any case, the behavior of a droplet thus crucially depends on the values of the characteristic frequencies and damping rates of the interface. In general, ω_n and β_n are functions of the mechanical properties of both the fluid and the interface. For Newtonian fluids, these properties are the densities of the inner (ρ_i) and the outer (ρ_o) fluids, and the viscosities of the inner (η_i) and the outer (η_o) fluids. For a clean interface between two immiscible pure fluids, the interface mechanics is fully characterized by the interfacial tension γ . However, in the presence of surface-active agents, the mechanical law of the interface can be much more complex and involve surface elasticity and viscosity. Ideally, the determination of ω_n and β_n for a given fluid system should involve three successive steps: (1) the chemical characterization of all the species that are present within bulk fluids as well as adsorbed at the interface; (2) the determination of the rheological properties of the interface resulting from the interactions between all these species; (3) the derivation of the interface-shape eigenmodes resulting from the specific mechanical laws of the interface under consideration. In practice, each of these steps is complex and involves a different scientific field: physico-chemistry, interfacial rheology, and fluid dynamics. Deriving one step from the preceding is not an easy task.

Connecting surface rheology (2) to chemical structure (1) shows the existence of two different origins of elasticity and viscosity of the interface.⁷ The first is related to the variations of the surface energy with the chemical composition of the interface⁸ and it can be considered to be of a *compositional* or a *thermodynamic* nature. Neglecting transfers of molecules between the bulk fluids and the interface, each increase (resp. decrease) of the interface area is associated with a decrease (resp. increase) of the interfacial surfactant concentration. This gives birth to a surface elasticity, which is usually called *Gibbs elasticity*. When surface-active molecules have time to adsorb or desorb during the duration of the process of interface dilatation (or compression), the Gibbs elastic modulus depends on the rate of molecule transfer. Moreover, this mass transfer causes fluid flows in the vicinity of the interface which generates viscous dissipation. Even if this dissipation is not located within the

interface, it gives rise to an apparent viscosity of the interface, which must not be confused with a true surface viscosity in the interpretation of experimental results. It is worth noting that compositional surface rheology is of an extrinsic nature as it depends not only on the interface properties but also on the physical properties and dynamics of the fluids that surround the interface. In addition, the corresponding elasticity and viscosity are only related to surface dilatation. The second origin of interfacial rheology is associated with interactions between adsorbed molecules. As the interface is deformed, the work of intermolecular forces under the change of the distance between molecules gives rise to a surface elasticity, whereas the motion of the molecules through the solvent and a possible irreversible reconfiguration of their relative positions and orientations can generate a surface viscosity. As these mechanisms take place within the interface and do not depend on bulk-fluid properties, they are considered to be of an *intrinsic* or a *rheological* nature. At variance with compositional rheology, intrinsic rheology is involved in both surface deformation at a constant area and area variation. It thus requires the introduction of a dilatation elastic modulus and a shear elastic modulus, as well as a dilatation viscosity and a shear viscosity.

Given a surface rheology (2), it is in principle possible to determine the interface dynamics (3). This requires to consider a coupled system of partial differential equations involving Navier–Stokes equations describing the dynamics of both bulk fluids, transport of species through the fluids, molecules transfers between the bulk fluids and the interface, and mechanical constitutional law of the interface. The interface-shape eigenmodes are found by solving this system after linearization under the assumption of small amplitude oscillations. Expressions for the frequency ω_n and the damping rate β_n are in general not explicit but under the form of the cancellation of a matrix determinant. Such solutions have been obtained for droplets constituted of two Newtonian fluids separated by a pure interface ($\gamma = cte$),^{3,9,10} an interface with intrinsic elasticity and viscosity,³ and an interface with Gibbs elasticity and intrinsic viscosity.^{11,12}

Various experimental methods have been developed to determine the rheological properties of interfaces: oscillating pendant drop,^{13–15} biconical disk interfacial rheometer,^{16,17} Langmuir trough with oscillating barriers,¹⁸ capillary pressure tensiometer,^{19,20} double wall-ring interfacial rheometer,^{21,22} and magnetic rod interfacial stress rheometer.²³ In general, the measured values of elasticity and viscosity are observed to depend upon the time scale at which the surface deformation occurs. Most of the time, these devices are operated at low frequency ($\omega/2\pi \lesssim 1$ Hz), in order to facilitate the accounting of bulk hydrodynamic effects in the determination of interfacial properties. Oscillations of a hemispherical bubble were used to investigate rheological interface properties in the range of 1–500 Hz.^{24–28} Despite the high-frequency range considered, because of the small size of the bubble ($d \approx 0.5$ mm), the forcing frequency was negligible compared to those of the shape eigenmode ($\omega_2/2\pi \approx 10^3$ Hz). The shape thus remained hemispherical, the interface experienced a uniform dilation, and inertia was considered to be negligible. Therefore, these measurements do not provide a characterization of the interface that is relevant for the study of droplet-shape eigenmodes. As far as we know, ref 29 is the only investigation of the rheological interface properties at a frequency matching that of droplet-shape eigenmodes. A droplet was suspended in air by acoustic levitation and forced to periodically oscillate in eigenmode 2.

Oscillation frequencies and damping rates were measured for droplets of various solutions of surfactant in water with concentrations below the critical micelle concentration. Rheological properties were determined by fitting the measured values of ω_2 and β_2 with the theoretical values based on Gibbs elasticity and dilatational viscosity, but without considering intrinsic elasticity.

Crude oil contains many components that can influence the rheology of the oil–water interface of droplets, such as asphaltenes, resins, solid particles, and acids.³⁰ Among them, asphaltenes play a major role because of their ability to form an irreversible network at the interface.³¹ An extensive literature has been devoted to low-frequency rheological characterization of the oil–water interface by considering either model fluids containing asphaltenes^{30,32–35} or crude oil.^{30,31,36,37,37–41} Most investigations made use of the oscillating pendant drop method,^{30–33,36–41} which gave access to the dilatational rheological properties, whereas a few works also used a double wall-ring interfacial rheometer, which measured shear properties.^{34,35} It turns out that oil–water interfaces display viscoelastic properties that depend on many parameters such as oil composition, chemical structure of asphaltenes, temperature, acidity, surface coverage (related to surface aging), and time scale (or frequency) of the interface deformation. Young interfaces with low surface coverage are expected to be dominated by compositional rheology as oscillating drop measurements are found³¹ in agreement with the Lucassen–van den Tempel (LVDT)⁴² model. Aged interfaces rather imply intrinsic elasticity.

Regarding low-frequency dilatational rheology based on oscillating drop experiments, as ref 32, numerous studies^{37–41} showed that the conservation modulus E' and the loss modulus E'' of the interface are in agreement with the behavior of a 2D gel near the gelation point^{43,44}

$$E' \propto E'' \propto \omega^z \quad (1)$$

where ω is the angular frequency of the oscillation and the exponent z is given by

$$z = \frac{2}{\pi} \tan^{-1} \left(\frac{E''}{E'} \right) \quad (2)$$

This behavior is generally attributed to the presence at the interface of asphaltene clusters of different sizes that result from the aggregation of nanoclusters. The corresponding interface rheology is therefore of an intrinsic nature. Recently, this mechanism was questioned in ref 45, where a model was proposed based on a compositional rheology. In this approach, the measured elastic moduli are predicted by an extension of the LVDT approach, which considers two surfactants having different diffusion and adsorption dynamics. This alternative interpretation gave rise to a vigorous debate.⁴⁶

Regarding low-frequency shear rheology, the conservation and loss moduli, G' and G'' , of oil–water interfaces with asphaltenes have been found to follow scaling law 1–2 as well.^{34,35} However, the given interpretation is different from that of a critical-gel behavior. Instead of cross-linking between asphaltenes, a mechanism of jamming is considered, which is described by a two-dimensional version of the soft-glassy rheology model (SGR) developed in refs.^{47,48} This model was first applied to interfacial shear rheology to describe micron-sized spheres,⁴⁹ Langmuir monolayers of polymers,⁵⁰ and carbon nanoparticles⁵¹ at fluid interfaces. The SGR model was then applied to asphaltenes in refs,^{34,35} with a noise temperature

$x = z + 1$ in the range between 1 and 2, which ensures that G' and G'' follows relations 1–2. Thus, although dilatational and shear moduli were found to exhibit the same scaling law, the critical-gel approach and the SGR model proposed to interpret them are based on different types of physicochemical interactions. It is however worth mentioning that both of them describe an intrinsic rheology.

With regard to high frequencies, we are not aware of any experimental studies of the rheology of crude oil–water interfaces. Determination of surface moduli at frequencies up to 100 Hz has been attempted by shifting the rheological curves obtained at low frequency for various temperatures³² by assuming a gel-type behavior, or for various surface pressures/aging times^{34,51} in the framework of the SGR model. However, no direct measurements at high frequencies were achieved so far.

The present work reports direct measurements of the shape-oscillation modes of a droplet of crude oil diluted in heptane immersed in water. The oscillating pendant drop method has been adapted to deal with high frequencies.⁵² A droplet of a few millimeters is attached to the tip of a capillary and forced to oscillate at a frequency up to 200 Hz by a periodic injection of a small amount of oil. The drop response is recorded by a high-speed video camera and the time-evolution of its shape is obtained by digital video processing. Eigenfrequencies and damping rates of modes 2–4 are then determined from the evolution of their amplitudes as a function of the forcing frequency. Compared to a droplet of pure heptane, both the frequencies and the damping rates are increased. This dynamic characterization is an important result that opens the way to the prediction of a droplet deformation in a turbulent flow⁶ involving complex interfaces. Furthermore, it also allows us to discuss the underlying rheology from theories relating surface viscosity and elasticity (2) to eigenfrequencies and damping rate (3). The results exhibit two regimes according to the age of the interface. The rheology of a moderately aged interface is similar at high and low frequencies, whereas that of an aged interface exhibits a different behavior. However, in both cases, intrinsic rheology plays a major role.

The article is organized as follows. We first present the fluid system under consideration and a characterization of the interface dilatational rheology at low frequency. Then, we describe the experimental determination of shape eigenmodes and draw conclusions about the influence of surface-active agents on the interfacial dynamics. Finally, we discuss the underlying rheology according to the interface age from the theory of eigenmodes.

■ MATERIALS AND LOW-FREQUENCY DILATATIONAL RHEOLOGY

Demineralized (Milli-Q) water is used as the outer phase. The inner phase is a mixture of light crude oil and *n*-heptane (p.a. grade, Sigma-Aldrich, used as purchased). The crude-oil concentration in the mixture was 10% (w/w). The physical properties of the crude oil used in this study are reported in Table 1, alongside with the saturate, aromatic, resin and asphaltene (SARA) analysis results of the 344+ fraction.

Using diluted crude oil as the drop phase is a deliberate choice. First, compared to undiluted oil, diluted crude oil has a viscosity low enough for the viscous stress not to screen the interfacial dynamics. The viscosity and the density of the diluted oil are substantially the same as those of *n*-heptane ($\eta_i = 0.4$ mPa s, $\rho_i = 680$ kg/m³ at 25 °C), allowing a direct comparison between the behaviors of diluted crude oil–water and heptane–water interfaces. Second, diluted crude oil is preferred to model fluids, such as asphaltene and resin solutions. This is motivated by the fact that crude oil is a very complex mixture, where thousands of

Table 1. SARA Analysis and Physical Properties of the Crude Oil

SARA analysis of the 344+ fraction	
saturates (% w/w)	47.5
aromatics (% w/w)	39.1
resins	12.6
asphaltenes	0.1
mass yield of the fraction (% w/w)	50.76
physical properties of the crude oil	
density at 15 °C (kg/m ³)	850
viscosity at 20 °C (Pa s)	9 × 10 ⁻³

components coexist and interact. The diluted crude oil–water interfacial rheology reflects this complexity.

The crude oil–water interface rheology has been characterized by the classic low-frequency oscillating pendant drop method,¹³ using a Tracker dynamic drop tensiometer from Teclis Scientific. Different interface ages have been considered, each of them corresponding to a quasistatic interfacial tension γ_e . Small sinusoidal volume oscillations ($\delta\theta \cos(\omega t)$) are imposed to a droplet that is attached to a capillary tube. At low frequency, the interface shape is controlled by a quasistatic balance between capillary and gravity forces, from which the dynamic interfacial tension $\gamma_d(t)$ can be determined. Denoting A the interface area, the surface elastic modulus E is obtained from

$$\frac{d\gamma_d}{d\ln A} = E \cos(\omega t + \phi) \quad (3)$$

The conservation modulus, $E' = E \cos(\phi)$, is associated to potential forces, whereas the loss modulus, $E'' = E \sin(\phi)$, is related to dissipative ones. As the oscillations correspond to a global inflation/deflation of the droplet, the interface experiences an almost uniform dilatation. In the case where the interface behavior is due to intrinsic rheology, $E_d = E'$ should therefore be interpreted as a surface dilation elasticity and $\eta_d = E''/\omega$ as a surface dilatation viscosity.

Experiments have been carried out at 25 °C. The amplitude of area variations was set to 5% and oscillation frequencies range between 0.1 and 1 Hz. This ensures linearity between droplet volume and area variations, as well as negligible inertial and viscous effects within bulk fluids. Figure 1a presents the evolution with the interface age of the static interfacial tension γ_e as well as the conservation and the loss moduli. The origin of age is taken at the end of the process of droplet formation at the tip of the capillary. As surface-active molecules can adsorb at the interface during droplet formation, the origin of age thus does not correspond to a heptane–water interface. Indeed, the first measurement performed at 114 s gives a value of γ_e equal to 27.6 mN/m, which is much lower than that measured with heptane alone ($\gamma_e = 47$ mN/m). Therefore, none of the present data corresponds to a young interface with a small surface coverage, and it is worth noting that in any case the conservation modulus E' is more than twice larger than the loss modulus E'' .

Figure 1 displays the existence of two distinct regimes of aging. The first regime starts a few hundred seconds after droplet formation until approximately five thousand seconds. It is characterized by a very slow decrease of γ_e from 27.6 to 24 mN/m and an increase of both E' and E'' as the power 0.25 of the interface age, their ratio remaining constant ($E''/E' \approx 0.41$). Beyond 5000 s, a second regime develops where the decrease of γ_e becomes steeper whereas the increase of E' is accelerated and E'' starts decreasing. From that point, the ratio E''/E' continuously decreases, becoming smaller than 1/3 for a time larger than 5.5×10^4 s.

As many previous studies^{32,34,35,37–41} have found that elastic moduli of oil–water interfaces containing asphaltenes did follow scaling law 1–2, this law has been evaluated on the present data. Figure 1b shows the evolution with age of the exponent z computed from the experimental values of E''/E' by eq 2. During the first regime, z is found constant and equal to 0.25, whereas during the second regime (≥ 5000 s) it decreases exponentially with age. Figure 2 shows the evolution of E' and E'' with frequency for two different ages within the first regime.

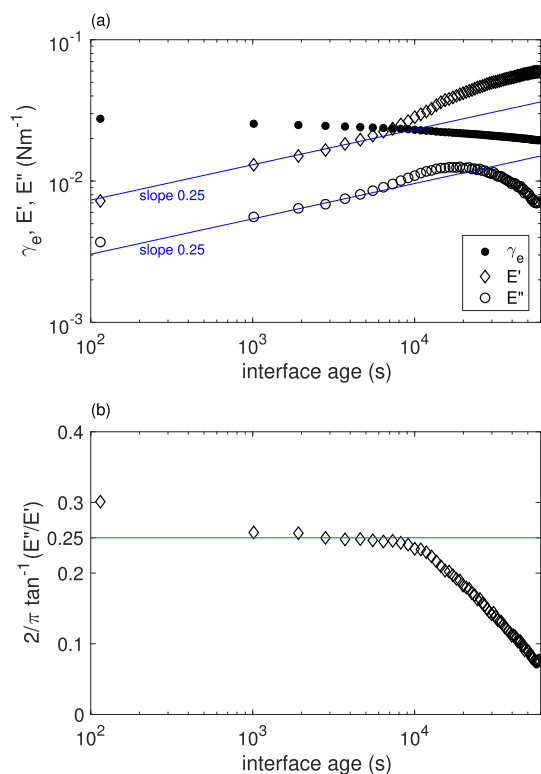


Figure 1. Evolution of interface properties with age measured by the oscillating drop method at a frequency $\omega/2\pi = 0.2$ Hz. (a) Static surface tension γ_e , conservation modulus E' , and loss modulus E'' . (b) Estimation of the exponent of the evolution of E' and E'' as a function of the frequency ω from eq 2.

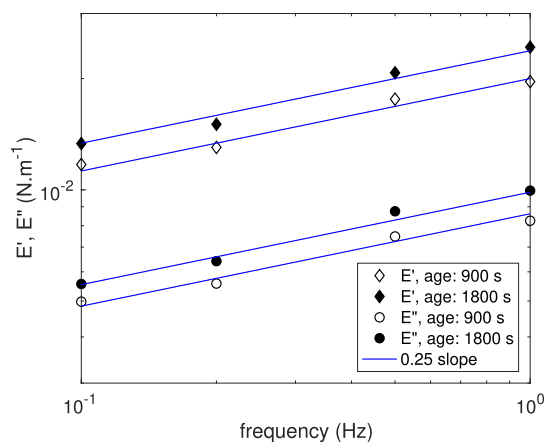


Figure 2. Evolution of interface moduli E' and E'' as a function of the frequency $\omega/2\pi$ for two different ages within the first regime (900 and 1800 s).

with eq 1, both moduli increase as ω^z with the value $z = 0.25$ given by eq 2.

This good agreement with scaling law 1–2 cannot, however, lead us to conclude about the underlying physicochemical mechanism. Let us discuss the interpretation in terms of critical-gel or SGR models by considering the features of the aging process. Describing the interface as a 2D-gel near its gelation point was proposed by ref 32 and considered in subsequent studies^{37–41} for the interpretation of dilatational interface elastic moduli of crude oil–water interfaces that were aged enough, typically for more than 14 hours, such as to be in thermodynamic equilibrium with the bulk phases. In the present study, as in ref 39, scaling law 1–2 is observed for moderately aged

droplets for which the aging process is not achieved yet, as γ_e is still slightly decreasing and especially both E' and E'' are significantly increasing. It is however not clear for us how the aging process, either by a continuous adsorption of asphaltenes at the interface or by an unceasing structuration of asphaltenes clusters, is consistent with the assumption of a 2D critical gel. The compatibility of the observed aging process with the SGR model is even more questionable. Assuming a constant composition of the interface, the SGR model only predicts⁴⁷ an evolution of the rheology for a noise temperature x lower than unity and, in this case, the loss modulus should decrease whereas the conservation modulus should remain constant. On the other hand, considering a continuous arrival of asphaltenes should increase the crowding and cause a decrease of x . However, during the first regime of aging, the exponent z characterizing the ratio E''/E' remains constant and corresponds to a noise temperature greater than unity $x = z + 1 = 1.25$. The SGR model seems therefore not consistent with the first regime of aging, whereas it is not in direct contradiction with the second regime where z tends toward zero.

At this stage, it is difficult to conclude about the nature of the aging process, which can be associated with either an evolution of the surface coverage governed by diffusion or a reorganization of the adsorbed molecules on the interface, or with both of them. Furthermore, the mechanisms causing the interface elastic moduli to follow scaling law 1–2, especially for a system which is still experiencing such an aging process, are still unknown. However, this scaling law seems to be a characteristic feature of the low-frequency rheology of crude oil–water interfaces. An important question is thus whether these dependences of the interfacial properties with the frequency is still valid in free droplet oscillations, which involve high frequencies and interface deformation implying both area dilation and shear. The next section will present investigations of the dynamics of a diluted crude-oil droplet oscillating at a high frequency in water.

■ HIGH-FREQUENCY DYNAMICS OF AN OSCILLATING DROPLET

Experimental Method. A pendant drop dynamic tensiometer is used to generate high-frequency droplet oscillations. It is a DSA 100 from Krüss equipped with an oscillating drop module (ODM) able to generate oscillations up to 200 Hz. Figure 3 shows a schematic of the setup. A syringe (1) is used to form an oil droplet at the end of a capillary immersed in water (4). A piezoelectric membrane (2'') mounted on a wall of the oil-storing cell (2) generates small droplet-volume oscillations at a given frequency ω . The droplet is illuminated by a light-emitting diode (LED) backlight panel (3) and recorded by a Photron APX high-speed camera (5) operated at a frame rate ranging between 60 and 2000 Hz, depending on ω . Then, the droplet shape is obtained at each instant by digital video processing of the images. Full details on the experimental technique are given in ref 52 where the method has been tested and validated for heptane droplets in water. Two conclusions of this previous work deserve to be mentioned. First, the limits of the linear regime of oscillations have been determined. Second, the roles of both gravity and attachment of the droplet to the capillary tip upon the eigenmodes of shape-oscillations have been shown to be negligible, provided the droplet size is large enough. The linear theory of a droplet oscillating around a spherical shape in the absence of gravity is thus relevant to interpret the results of the present study.

Small droplet-volume oscillations drive interface-shape oscillations. In order to be analyzed, shape oscillations need to be decomposed into spherical harmonics, which correspond to the eigenmodes of oscillations. As the droplet remains axisymmetric, its shape at each instant is fully characterized by the local radial position r of the interface as a function of polar

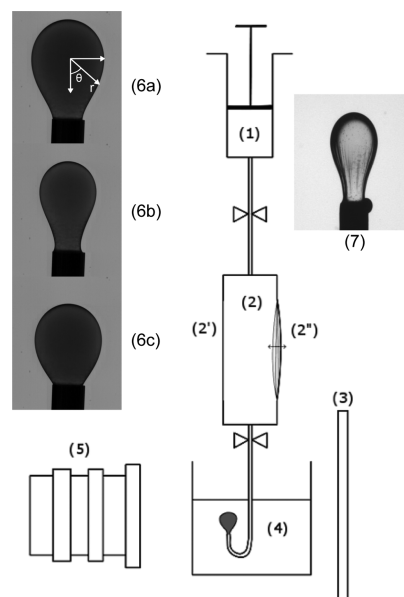


Figure 3. Experimental setup: (1) feeding syringe, (2) drop phase storing cell, (2') glass window, (2'') piezoelectric membrane, (3) LED backlight panel, (4) droplet formed at the tip of capillary tube immersed in water stored in a parallelepipedic optical-grade glass cell, (5) high-speed camera; (6) T2B interface before compression (a) after shrinkage (b) and just before oscillations (c). (7) Visualization of wrinkles on a shrunk interface.

angle θ (see Figure 3). The local radius of the interface is thus written as

$$r(t) = a \left(A_0(t) + \sum_{n=2}^N A_n(t) P_n(\cos(\theta)) \right) \quad (4)$$

where a is the radius of the sphere of same volume $\vartheta = 4/3\pi a^3$ as that of the droplet, $A_0(t)$ stands for the volume variation, and $A_n(t)$ is the instantaneous dimensionless amplitude of spherical harmonic n , which is defined by Legendre polynomial P_n . Rigorously, the summation should expand to infinity. However, it turns out that it is sufficient to stop to harmonic 10 to accurately describe the experimental shapes. At each instant, the A_n are determined by fitting the experimental droplet contours using eq 4 with $N = 10$. As the equilibrium shape of the droplet is not spherical, the time average is subtracted from each $A_n(t)$ signal, so that only the fluctuating part $\Delta A_n(t)$ is kept. In the following, we present results concerning the three first modes of shape oscillations, which correspond to $n = 2, 3$, and 4. Figure 4 illustrates the time evolution of $\Delta A_n(t)$. As oscillations lie in the linear regime, we observe perfect sinusoidal functions $\Delta A_n(t) = \delta A_n \cos(\omega t + \phi)$, from which we can determine the peak amplitude δA_n within an accuracy of 5%. This procedure is repeated for various forcing frequencies ω in order to obtain a resonance curve $\delta A_n(\omega)$ for each mode. Owing to the design of the ODM, the amplitude of the oscillating forcing volume $\delta\vartheta$ cannot be maintained constant as ω is varied. Therefore, each $\delta A_n(\omega)$ needs to be divided by the relative amplitude of volume variations: $\tilde{A}_n(\omega) = \delta A_n(\omega) / (\delta\vartheta(\omega) / \vartheta)$.

Various Types of Interfaces Considered. Three types of interfaces are considered, which differ by their state of aging (see Table 2). Type T0 is the reference case of a droplet of heptane. Type T1 corresponds to a diluted crude-oil droplet of age 1200 s, which therefore belongs to the first aging regime displayed in Figure 1. Considering older interfaces belonging to the second

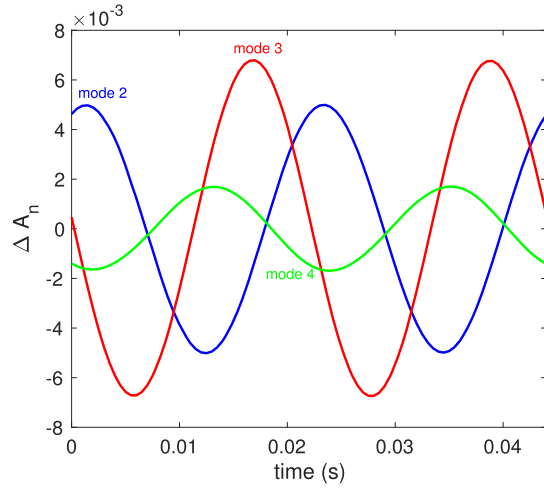


Figure 4. Time evolution of the amplitudes of spherical harmonics characterizing interface-shape oscillation (example for T1 interface).

regime of aging was more problematic. Because of a lack of a regulation system of the volume, the DAS 100 tensiometer did not allow one to maintain a pendant droplet for 5000 s or more. To overcome this limitation, type T2 has been obtained by provoking an artificial aging of the interface (pictures 6a–c in Figure 3), based on the idea that reducing the interface area increases the concentration of adsorbed molecules in a similar way as aging. A droplet is formed at the capillary tip and let in contact with water during initial aging time Δt_1 . Then, the droplet is shrunk by sucking a given amount of oil until wrinkles appear (picture 7 in Figure 3). Then, the droplet volume is slightly increased back, just enough for the wrinkles to disappear. Finally, the droplet is let to relax for a duration Δt_2 before starting oscillations. Moderate initial aging time and relaxation time are applied to type T2A ($\Delta t_1 = 1200$ s, $\Delta t_2 = 300$ s), whereas longer ones are applied to type T2B ($\Delta t_1 = 3600$ s, $\Delta t_2 = 1200$ s). It is important to stress that, if reducing the interface area is very likely to increase surface coverage, we ignore if it causes a reorganization of surfactants at the interface which is similar to aging. For that reason, we will not claim that interfaces T2 really correspond to the second regime of aging identified in Figure 1. Type T2 will be used to probe whether results obtained with type T1 still hold for interfaces having experienced a more complex history. In the following, type T2 will be referred as to “artificially aged interfaces”.

Resonance Curves of Shape Oscillations. Figures 5–8 display the response in amplitude of modes 2–4 as a function of the forcing frequency ω for the various types of interfaces under consideration. Symbols correspond to experimental data.

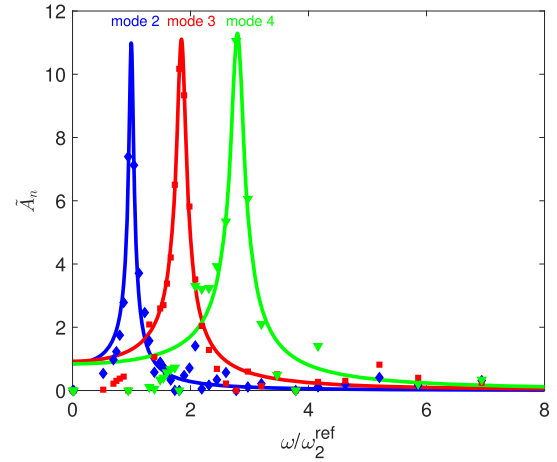


Figure 5. Amplitudes \tilde{A}_n of interface modes 2–4 as a function of the forcing frequency for a drop of heptane in water (type T0). Symbols: measurements. Lines: best fit of each peak by a harmonic oscillator (eq 5).

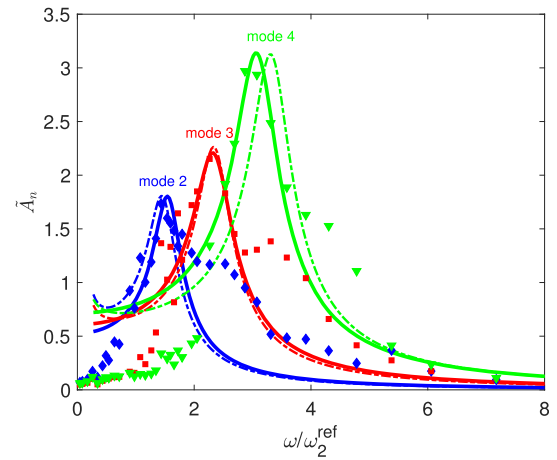


Figure 6. Amplitudes \tilde{A}_n of interface modes 2–4 as a function of the forcing frequency for a moderately aged diluted crude-oil droplet in water (type T1). Symbols: experimental data. Continuous lines: best fit of each peak by a harmonic oscillator (eq 5). Dashed lines: prediction from theory by using values of interface rheological properties extrapolated from low-frequency characterization: $E_s = 2E_d = 2E'^{\text{extra}}(\omega)$ and $\eta_s = 2\eta_d = 2E''^{\text{extra}}(\omega)/\omega$.

Continuous lines show the theoretical resonance curve $\tilde{A}_n(\omega)$ of a linear harmonic oscillator

$$\tilde{A}_n(\omega) = \frac{2\beta_n^{\text{exp}} \omega_n^{\text{exp}} \tilde{A}_n^{\text{max}}}{\sqrt{(\omega_n^{\text{exp}2} - \omega^2)^2 + 4\beta_n^{\text{exp}2} \omega^2}} \quad (5)$$

Table 2. Various Types of Interfaces Considered in High-Frequency Experiments

interface type	T0	T1	T2A	T2B
inner fluid	heptane	diluted crude oil + heptane	diluted crude oil + heptane	diluted crude oil + heptane
outer fluid	water	water	water	water
droplet diameter (mm)	4.48	3.73	3.06	3.27
aging time Δt_1 (s)		1200	1200	3600
contraction/expansion cycle	no	no	yes	yes
relaxation time after expansion Δt_2 (s)			300	1200
static interfacial tension γ_c (mN/m)	47	25	20	20

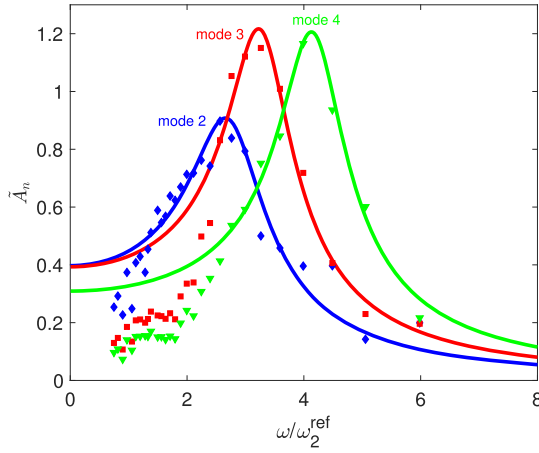


Figure 7. Amplitudes \tilde{A}_n of interface modes 2–4 as a function of the forcing frequency for an artificially aged crude-oil droplet in water (type T2A). Symbols: measurements. Continuous lines: best fit of each peak by a harmonic oscillator (eq 5).

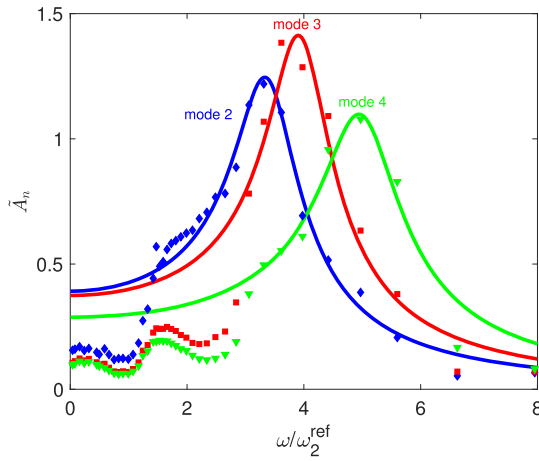


Figure 8. Amplitudes of interface modes 2–4 as a function of the forcing frequency for an artificially aged crude-oil droplet in water (type T2B). Symbols: measurements. Continuous lines: best fit of each peak by a harmonic oscillator (eq 5).

where the angular frequency ω_n^{exp} , the damping rate β_n^{exp} , and the maximum at resonance \tilde{A}_n^{max} have been adjusted to provide the best fit of the peak of each mode n . Experimental frequencies and damping rates are reported in Tables 3–6, together with the

Table 3. Frequencies and Damping Rates of Eigenmodes of a 4.48 mm Heptane Drop in Water (Type T0)

mode	ω^{exp} (rad/s)	ω^{ref} (rad/s)	β^{exp} (s^{-1})	β^{ref} (s^{-1})
2	151	154	5.85	4.67
3	279	289	11.61	8.82
4	423	440	15.81	13.90

Table 4. Frequencies and Damping Rates of Eigenmodes for a Moderately Aged Diluted Crude-Oil Droplet in Water (Type T1)

mode	ω^{exp} (rad/s)	ω^{ref} (rad/s)	β^{exp} (s^{-1})	β^{ref} (s^{-1})
2	230	146	34	5.62
3	345	275	48	10.62
4	453	419	52	16.75

Table 5. Frequencies and Damping Rates of Eigenmodes for an Artificially Aged Diluted Crude-Oil Droplet in Water (T2A)

mode	ω^{exp} (rad/s)	ω^{ref} (rad/s)	β^{exp} (s^{-1})	β^{ref} (s^{-1})
2	490	175	110	7.60
3	580	328	95	14.35
4	735	500	95	22.64

Table 6. Frequencies and Damping Rates of Eigenmodes for an Artificially Aged Diluted Crude-Oil Droplet in Water (T2B)

mode	ω^{exp} (rad/s)	ω^{ref} (rad/s)	β^{exp} (s^{-1})	β^{ref} (s^{-1})
2	540	158	86	6.76
3	628	297	84	12.75
4	795	452	105	20.11

theoretical values ω_n^{ref} and β_n^{ref} obtained by assuming an interface described by a constant interfacial tension.³ The considered values of γ_e are given in Table 2 and correspond to the static interfacial tension measured for each interface type. These reference frequencies and damping rates thus only account for the presence of surface-active agents through the values of the interfacial tension but ignore the complex rheology of the interface.

The case of the heptane droplet (T0) is used to determine to which extent the theory of a free droplet in the absence of gravity is relevant to interpret the present experiments. As expected, it is in fairly good agreement with the theory of a pure interface. The resonance curve of each mode (Figure 5) shows a narrow peak. The experimental values of the frequencies are within 2% of the theoretical values for mode 2 and 4% for mode 4, whereas the discrepancy on the damping rate is about 20% (Table 3). As discussed in ref 52, the larger discrepancy in β_n can be attributed to the effect of the attachment of the droplet to the capillary. In the following, these discrepancies will be considered as reasonable estimates of overall uncertainties made in the determination of ω_n and β_n for interfaces of types T1 and T2.

Let us now consider a moderately aged interface (T1). The resonance curves (Figure 6) are shifted toward higher frequencies whereas the peaks are much broader. Table 4 shows that experimental frequencies are larger than reference ones by 57% for mode 2, 25% for mode 3, and 8.1% for mode 4. Moreover, experimental damping rates are larger than reference ones: six times larger for mode 2, four times for mode 3, and three times for mode 4.

The effect of surface-active agents is even more stronger for artificially aged interfaces. Interfaces T2A (Figure 7) and T2B (Figure 8) show very similar resonance curves. The peaks strongly moved toward high frequencies and are very much wider so that they partly overlap. For mode 2, the experimental eigenfrequencies are about three times larger than the reference frequency, whereas the experimental damping rates are more than 12 times larger than the reference value (Tables 5 and 6).

We can therefore conclude that surface-active agents that are present in crude oil significantly change the mechanical behavior of the interface at frequencies around 100 Hz. As well-defined resonance peaks are detected for crude oil–water interfaces of any age, the present method is able to characterize the dynamics of shape oscillations of droplets having a complex interface. The eigenfrequencies and damping rates of shape eigenmodes can therefore be directly measured. Moreover, as eigenfrequencies

are in general more sensitive to surface elasticity, whereas damping rates are more influenced by surface viscosity, the present results suggest that the diluted crude oil–water interface features significant viscoelastic properties, which depend on the aging process. In the next section, we attempt to infer the surface elasticities and viscosities from the resonance curves and discuss the relation between low- and high-frequency interfacial rheology.

■ DISCUSSION ON INTERFACIAL RHEOLOGY

Theoretical Background. Our objective is to determine the elasticity and the viscosity of the interface from the measured eigenfrequencies and damping rates. This can be done by solving the coupled dynamic equations for the fluids and the interface. However, it requires first to assume a model that describes the interfacial rheology. Let us start by reviewing the various possible origins of the viscoelastic properties of the interface.

The first cause of complex interfacial rheology is of a compositional nature and only concerns dilatation. It arises from the fact that surface energy γ depends upon the surface concentration of surface-active agents and gives birth to Gibbs elasticity. For a single surfactant at surface concentration Γ , it writes: $E_{\text{Gibbs}} = -d\gamma/d\ln \Gamma$. (For multiple surfactants we have to consider the sum of all contributions to the Gibbs elasticity.) For an insoluble surfactant, the number of molecules adsorbed on the surface is constant and the variations of concentration are simply related to the interface area A by $d\ln \Gamma = -d\ln A$. In this case, the conservation modulus E' measured in low-frequency oscillating pendant drop experiments is thus equal to E_{Gibbs} . When molecule transfer occurs between the interface and the droplet bulk, E' is in general lower than E_{Gibbs} . It decreases when transfer becomes faster as the magnitude of concentration variations during an oscillating period is attenuated. The time scale of transport of surfactant molecules through the bulk is controlled by diffusion in the vicinity of the interface and writes:

$\tau_{\text{diff}} = \frac{1}{D} \left(\frac{\partial \Gamma}{\partial C} \right)^2$, where C and D are respectively the surfactant concentration and diffusion coefficient in the droplet fluid. The dimensionless group $\lambda = (\omega \tau_{\text{diff}})^{-1/2}$ is then introduced¹¹ to compare the time scale of diffusion to the oscillating period, the case $\lambda = 0$ corresponding to negligible molecule transfer. The effective compositional elasticity is thus controlled by both E_{Gibbs} and λ . As molecule transfers are associated with a dissipative motion in the fluid, a loss modulus is also measured in low-frequency oscillating pendant drop experiments when $\lambda \neq 0$, even in the absence of any real interface viscosity. The same mechanism can be responsible for an increase of the damping rate of droplet shape eigenmodes at a high frequency.

The second cause of interfacial viscoelasticity is related to interactions between adsorbed molecules, which give rise to intrinsic surface elasticity and viscosity. The interface should thus be considered as a two-dimensional viscoelastic material, which is characterized by four physical parameters: a dilatational elasticity E_d , a shear elasticity E_s , a dilatational viscosity η_d , and a shear viscosity η_s .

Assuming small amplitude oscillations, the dynamic equations describing the droplet oscillations can be linearized. The eigenfrequency and the damping rate of each mode are then determined by cancelling the determinant of a matrix, which leads to solve a transcendental equation. This equation was first derived in two seminal works. First, ref 3 considered the case of an elastic interface involving interfacial tension (γ_c), dilatational and shear elasticities (E_d , E_s), as well as dilatational and shear

viscosities (η_d , η_s). Then, ref 12 addressed the case of viscoelastic interface involving compositional rheology (E_{Gibbs} , λ) and intrinsic viscosity (η_d , η_s). By completing the determinant of ref 12 by the terms corresponding to intrinsic elasticity derived by ref 3, the general equation for an interface including compositional rheology as well as both intrinsic elasticity and viscosity is obtained (see Appendix I for details). In what follows, this equation is solved numerically to determine the values of ω_n and β_n .

Moderately Aged Interface (T1). We start by analyzing moderately aged interface T1, which belongs to the first regime of aging identified from low-frequency dilatational rheology. In this regime, interfaces are still aging but yet show a significant viscoelastic rheology with $E' > E''$. For oscillating frequencies ω in the range from 0.63 to 6.3 rad/s, both moduli have been found to evolve as $\omega^{0.25}$. In order to assess whether this behavior still holds at high frequency, the functions $E'(\omega)$ and $E''(\omega)$ determined at low frequency (Figure 2) have been extrapolated to higher frequencies by assuming that the $\omega^{0.25}$ law is still valid. Extrapolated values evaluated at the peak frequency of the resonance curves, $E'^{\text{extra}}(\omega_n^{\text{exp}})$ and $E''^{\text{extra}}(\omega_n^{\text{exp}})$, are reported in Table 7, where E''^{extra} has been divided by ω_n^{exp} to allow its

Table 7. Conservative and Loss Interface Moduli Extrapolated from Low-Frequency Dilatational Rheology Measurements for a Moderately Aged Diluted Crude Oil–Water Interface (T1)

mode	ω^{exp} (rad/s)	E'^{extra} (N/m)	$E''^{\text{extra}}/\omega^{\text{exp}}$ (N·s/m)
2	230	0.053	9.5×10^{-5}
3	345	0.059	7.0×10^{-5}
4	453	0.063	5.7×10^{-5}

interpretation as a surface viscosity. Values of $E'^{\text{extra}}(\omega_n^{\text{exp}})$ are found to be of the order of 0.05 N/m whereas those of $E''^{\text{extra}}(\omega_n^{\text{exp}})/\omega_n^{\text{exp}}$ are of the order of 10^{-4} N·s/m.

The model of the interface described above involves six a priori unknown parameters (E_{Gibbs} , λ , E_d , E_s , η_d , η_s). It is too much to attempt a brute-force determination of the parameters by searching for the values that provide the best fit of the experimental values of ω_n and β_n . We thus adopt a step-by-step approach.

Considering only static interfacial tension, the eigenfrequency of mode 2 should be $\omega_2^{\text{ref}} = 146.5$ rad/s, whereas the measured value is $\omega_2^{\text{exp}} = 230$ rad/s. Such an important increase in the frequency is expected to be the signature of a surface elasticity. Let us first assess whether it can be due to a compositional elasticity. Figure 9 shows the theoretical value of ω_2 as a function of E_{Gibbs} for various values of λ . It turns out that ω_2 is not a monotonic function of E_{Gibbs} and its value never exceeds ω_2^{ref} by more than 3%. In the absence of molecule transfer between the bulk and the interface ($\lambda = 0$), ω_2 first increases from the initial value 146.5 rad/s up to reach a maximum at 149.8 rad/s for $E_{\text{Gibbs}} = 1.2 \times 10^{-3}$ N/m; then it continuously decreases as E_{Gibbs} further increases. Accounting for molecule transfer ($\lambda > 0$) simply moves the maximum to the right and reduces its magnitude. It is worth mentioning that, in the absence of molecule transfer, the effect of the Gibbs elasticity E_{Gibbs} is exactly the same as that of an intrinsic dilatational elasticity E_d . In other words, the function $\omega_2(E_{\text{Gibbs}})$ for $\lambda = 0$ is the same as the function $\omega_2(E_d)$, which does not depend on λ . This leads to an important conclusion. The strong increase in ω_2 cannot be the result of only a compositional rheology. More generally, it can

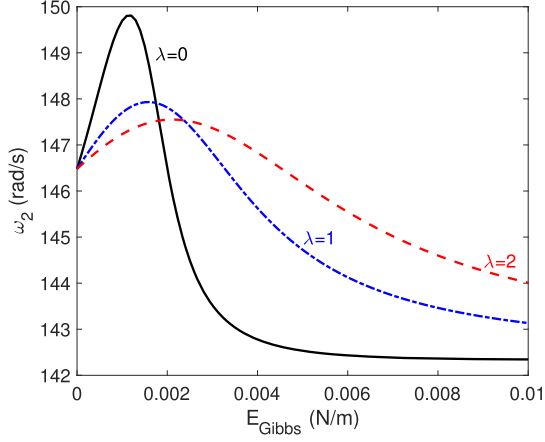


Figure 9. Mode-2 frequency as a function of the Gibbs (or intrinsic dilatational) surface elasticity (physical parameters of case T1 and $E_s = \eta_d = \eta_s = 0$).

neither be explained by only considering any kind of dilatational elasticity. Because we are dealing with high frequencies, we will set $\lambda = 0$ in what follows. This implies that there will be no more distinction between E_{Gibbs} and E_d regarding the comparison between the prediction of the model and experimental resonant curves.

Figure 10 shows ω_2 as a function of the shear elasticity E_s for various dilatational elasticities E_d . The function $\omega_2(E_s)$ for $E_d = 0$

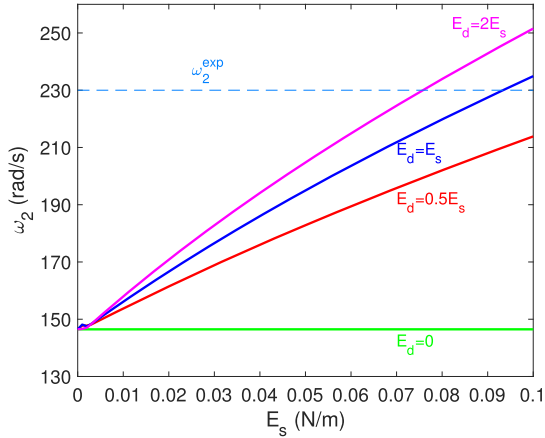


Figure 10. Mode-2 frequency as a function of the shear surface elasticity for various dilatational surface elasticities (physical parameters of case T1 and $E_{\text{Gibbs}} = \lambda = \eta_d = \eta_s = 0$).

is flat. Taken together, results of Figures 9 and 10 show that increasing either the dilatational or the shear elasticity while the other one is set to zero does not lead to a significant increase of ω_2 . However, when neither of the moduli is negligible, ω_2 turns out to be an increasing function of both E_d and E_s . Moreover, when E_d and E_s are of the same order of magnitude, the value $\omega_2^{\text{exp}} = 230$ rad/s can be reached for an elasticity of the order of the extrapolated conservation modulus $E^{\text{extra}}(\omega_2^{\text{exp}}) = 0.053$ N/m.

Figure 11 shows the theoretical damping rate β_2 of mode 2 as a function of the dilatational viscosity η_d for various shear viscosities η_s and $E_s = E_d = 0.053$ N/m. The value of β_2 are increasing functions of both η_d and η_s . Similar to what was observed for the effect of elasticity upon frequency, it is possible to retrieve the experimental damping rate, $\beta_2^{\text{exp}} = 34$ s⁻¹, with

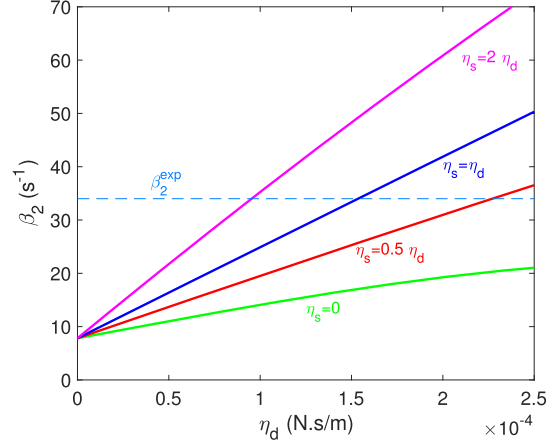


Figure 11. Mode-2 damping rate as a function of the dilatational surface elasticity for various shear surface viscosities (physical parameters of case T1 and $E_{\text{Gibbs}} = \lambda = 0$, $E_s = E_d = 0.053$ N/m).

values of both viscosities that are close to the extrapolated value $E^{\text{extra}}(\omega_2^{\text{exp}})/\omega_2^{\text{exp}} = 9.5 \times 10^{-5}$ N·s/m.

Assuming a viscoelastic interface with both (1) an elastic dilatational elasticity and a shear elasticity of the same order and (2) a dilatational viscosity and a shear viscosity of the same order is therefore compatible with the observed shape-oscillation dynamics. Moreover, the measured eigenfrequency and damping rate of mode 2 can be recovered with values of elasticities and viscosities close to the values obtained by extrapolating the conservation and loss modulus measured at a low frequency by assuming that the $\omega^{0.25}$ law is still valid at a high frequency. Unfortunately, there is no unique set of parameters (E_d , E_s , η_d , η_s) that leads to the experimental values ω_2^{exp} and β_2^{exp} . For example, Figure 10 shows that ω_2^{exp} can be reached for two different values of E_s depending on whether E_d is assumed to be equal to E_s or twice as large. If we consider that the functions $E'(\omega_2)$ and $E''(\omega)$ obtained from low-frequency dilatational rheology are valid in the whole range of frequency investigated in this work, the dilatational elasticity and viscosity should be given by

$$E_d(\omega) = E^{\text{extra}}(\omega) \propto \omega^{0.25} \quad (6)$$

$$\eta_d(\omega) = E^{\text{extra}}(\omega)/\omega \propto \omega^{-0.75} \quad (7)$$

However, if the ratios E_s/E_d and η_s/η_d are known to be of order 1, their exact values remain undetermined. To go further, the resonance curves $\tilde{A}_n(\omega)$ of modes 2–4 have been computed by the following method. First of all, the ratios E_s/E_d and η_s/η_d are set to a given value. For a given forcing frequency ω , the values of E_d and η_d are determined by eqs 6 and 7, whereas those of E_s and η_s are given by the prescribed ratios. The dynamic parameters ω_n and β_n are computed by solving the transcendental equation which describes the dynamics for that given set of surface viscosity and elasticity. Then, the mode amplitude \tilde{A}_n is calculated by using eq 5. Finally, the resonance curves $\tilde{A}_n(\omega)$ are obtained by doing the same calculation for all ω .

The best results, obtained for $E_s/E_d = 2$ and $\eta_s/\eta_d = 2$, are reported in Figure 6 (dashed lines). (Other examples of theoretical resonant curves are shown in Figure 14 of Appendix II.) Regarding that the only adjustable parameters are the ratios E_s/E_d and η_d/η_s , the agreement with the experimental curves is remarkable. Only a slight discrepancy on the peak frequency of mode 4 is to be noted. Except from that, the peak frequency and

the peak width of all three modes are very well reproduced. We can therefore conclude that the evolutions of the surface elasticity as $\omega^{0.25}$ and of the surface viscosity as $\omega^{-0.75}$ are valid for the frequency range of the three modes.

Regarding moderately aged interface T1, the results thus indicate that the rheology of the crude oil–water interface, which controls droplet-shape oscillations in the range of frequencies between 10 and 80 Hz, is not different from that governing quasistatic oscillations at frequencies smaller than 1 Hz. The interface behaves as a 2D viscoelastic material with shear elasticity and viscosity that are of the same order of magnitude as their dilatational counterparts and are in agreement with scaling law 1–2.

The fact that the best fit of the experimental resonant curves is obtained for $E_s > E_d$ deserves discussion. If we interpret the observed rheological behavior as the existence of real 2D membrane, its material would be auxetic, which would be hardly believable and in conflict with our assumption of 2D isotropy. However, even if we consider that there exists a membrane of constant composition, its structure is three-dimensional at the molecular level and there is no reason to extend the isotropy property of the interface plane in the normal direction. When the in-plane area increases, its thickness may decrease because of rearrangement or rotation of asphaltene clusters: we can therefore conclude nothing about the volume variation of this material. That being said, it is also possible that the composition of the interface changes as its area varies. When oscillations are rapid ($\lambda = 0$), the number of surface-active molecules at the interface remains constant but more or less water or oil molecules can occupy the spaces between them. Thus, because either the organization of the surfactant in the direction normal to the interface or composition may change during the oscillations, the interface is not a real 2D material and there is, in principle, no reason to reject a description involving an effective 2D rheology with $E_s > E_d$. However, even if the best fit is obtained with $E_s > E_d$, the discrepancy with $E_s = E_d$ is not so large. It is therefore reasonable to limit our conclusion to the fact that E_s and E_d are of the same order.

Once an effective rheology has been inferred from the dynamics, the underlying physicochemical mechanisms can be discussed. Regarding shear elasticity and viscosity, there is no doubt that they are of an intrinsic nature and imply interactions between adsorbed molecules or molecules clusters. However, it is difficult to conclude whether these interactions imply molecular bounds, like in a gel, or steric effects, like in a soft glassy material. Regarding dilatational rheology, the question of its compositional or intrinsic nature is more complex and requires to distinguish between elasticity and viscosity. As already mentioned, the results of the present model do not make any difference between an intrinsic dilatational elasticity and a compositional Gibbs elasticity. There is no reason to think that Gibbs elasticity is null, especially at a high frequency for which variations of surface concentration are expected to be directly related to area variations. The observed value of E_d could thus a priori be due to any combination of compositional and intrinsic contributions. Furthermore, as we have considered that oscillations are rapid compared to diffusion time ($\lambda = 0$) and thus assumed insoluble surfactant, all damping effects modeled by intrinsic viscosities η_s and η_d do not include any effect because of changes in interface composition. However, if there existed a dissipation related to an irreversible process associated to periodic changes in interface composition, this effect would be imbedded in the observed value of η_d . Because values of

dilatational elasticity and viscosity are found to be strongly correlated to their shear counterparts, we are prone to think that dilatational rheology is predominantly of an intrinsic nature. Having no certainty about the physicochemical structure of the interface, we cannot preclude a coupling between compositional and intrinsic mechanisms that would lead to correlate the values of elasticity and viscosity.

Artificially Aged Interface (T2). As indicated by the large peak frequencies of the resonance curves plotted in Figures 7 and 8, T2 interfaces exhibit a large elasticity. According to the way they are produced, it is reasonable to think that their coverage rate is close to the interface saturation. We a priori expect them to be representative of ages far beyond the first regime of aging, which ends at 5000 s. However, because of their complex history a direct comparison between low- and high-frequency rheological characterization is therefore not possible for them. As a consequence, we have no clue to estimate either the values of elasticity and viscosity at high frequency or their possible dependence on frequency. Therefore, we cannot use the same method as for T1 interfaces where the resonance curves have been computed by using expected values of E_d and η_d . We shall thus attempt to infer rheological properties from measured values of ω_n^{exp} and β_n^{exp} .

On the basis of what we learnt from the T1 interface, we attempt to describe T2 interfaces by a two-dimensional viscoelastic rheology. Here, we present results obtained by keeping the aspect ratios that gave the best fit for interface T1: $E_s/E_d = 2$ and $\eta_s/\eta_d = 2$. Note that similar conclusions are obtained for other ratios of order 1. (In particular, the results obtained for $E_s/E_d = 1$ and $\eta_s/\eta_d = 1$ are provided in Figures 15 and 16 of Appendix II.) The two remaining free rheological parameters, E_d and η_d , are then adjusted so that the values of ω_n and β_n obtained by solving the dynamic equations match the experimental values ω_n^{exp} and β_n^{exp} reported in Tables 5 and 6. The determination of E_d and η_d is carried out independently for each mode of interfaces T2A and T2B. Figure 12 shows the moduli $E' = E_d$ and $E'' = \omega_n \eta_d$ obtained by this method as a function of the frequency. As three eigenmodes have been investigated, three measurements points are available for each modulus and each interface type. The moduli E' and E'' of mode 2 of T2A and T2B interfaces (first points from the left in Figure

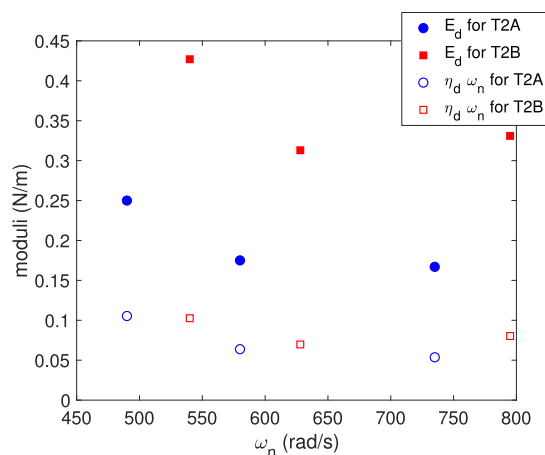


Figure 12. Conservation ($E' = E_d$) and loss ($E'' = \omega_n \eta_d$) moduli determined by matching the frequency and damping predicted by oscillation theory to measured values for interfaces of types T2A and T2B, assuming $E_s = 2E_d$ and $\eta_s = 2\eta_d$.

12) are found to be 5–10 times larger than those of T1 interface. However, the range of frequencies available for T2 interface spreads from 490 rad/s (ω_2^{exp} of T2A) to 795 rad/s (ω_4^{exp} of T2B), above the range of the T1 interface ($230 \leq \omega_n^{\text{exp}} \leq 453$ rad/s). We must keep in mind that the investigation of T2 interfaces thus differs from that of the T1 interface by both the aging and the frequency range.

The conservation modulus of T2B interface, which is older, is about twice as large as that of the T2A interface. However, the evolution of elasticity with frequency is similar for the two types of interfaces. We observe a significant decrease between 500 and 600 rad/s and then a plateau between 600 and 800 rad/s. On the other hand, the loss moduli of T2A and T2B interfaces have similar values and do not display any significant evolution with ω_n . These trends are clearly not in agreement with the $\omega^{0.25}$ increase of both moduli observed for the T1 interface. The disparity of behavior with the T1 interface is confirmed by Figure 13, which shows the modulus ratio E''/E' as a function of

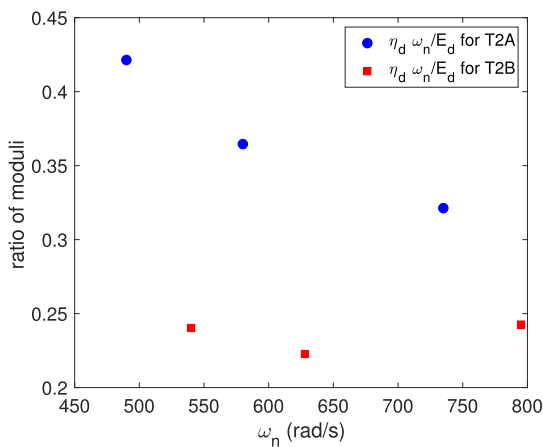


Figure 13. Ratio of loss modulus to conservation modulus from values presented in Figure 12 for interfaces of types T2A and T2B.

frequency. Regarding T2A, the ratio starts from a value ($E''/E' = 0.42$ at $\omega_n = 490$ rad/s) close to that of T1 ($E''/E' = 0.41$), but it then decreases strongly to reach $E''/E' = 0.32$ at $\omega_n = 735$ rad/s. Regarding T2B, E''/E' is approximately constant and equal to 0.24 throughout the available frequency range ($540 \leq \omega \leq 795$ rad/s).

The major discrepancy between the interfacial rheology of T1 and T2 interfaces lies in the different evolution of the moduli with the frequency. T2 interfaces are not compatible with scaling law 1–2 for frequencies larger than 500 rad/s. Results obtained with the T2A interface show that this might result from only the difference in the considered range of frequency, as the results are compatible with the $\omega^{0.25}$ power law and a constant modulus ratio ($E''/E' \approx 0.4$) for ω below 500 rad/s and a decrease of elasticity beyond. This interpretation cannot be confirmed by high-frequency T2B-interface results, which start at 540 rad/s, where the modulus ratio is already as small as 0.26. We can thus not definitively conclude whether the differences in the viscoelastic properties of T1 and T2 should be ascribed to either the frequency range or the aging process, or to both of them.

CONCLUSIONS

The dynamic response to periodic forced oscillations of a diluted crude-oil droplet in water has been investigated at a low

frequency by classical dilatation experiments and, for the first time, at a high frequency by exciting inertial modes of shape oscillations.

For frequencies $\omega/2\pi$ lower than 1 Hz, the droplet shape is controlled by a simple quasistatic balance between buoyancy and surface tension, providing a direct characterization of the dilatational rheology of the interface by the determination of the conservation modulus E' and the loss modulus E'' . Because of the process of formation, the coverage rate of the droplet by surfactants is significant and its interface shows from the beginning a substantial viscoelastic behavior with $E' > E''$. However, the interface is not at equilibrium and an aging process is observed, which displays two successive stages. A first regime is observed for aging times between a few hundred and 5000 s, where both moduli increase with time but their ratio remains constant. In addition, E' and E'' both increase with the forcing frequency as ω^z , with $z = \frac{2}{\pi} \tan^{-1}\left(\frac{E''}{E'}\right) = 0.25$. Such a scaling law has been reported in many previous works involving crude oil either for surface dilatational moduli^{32,37–41} and interpreted as a 2D critical gel, or for shear moduli^{34,35} and interpreted as a 2D soft glass material in the framework of the SGR model. In the present case, because of the aging process that is taking place, it is not clear whether any of these interpretations can apply. However, this scaling law seems to be a characteristic of crude oil or model fluids involving asphaltenes and resins. A second regime of aging occurs at a larger time where the conservation modulus increases faster with age, whereas the loss modulus decreases, indicating that surface elasticity becomes more and more predominant.

For frequencies between 10 and 200 Hz, inertial modes of droplet shape oscillations are excited. The interface thus undergoes oscillations which result from the interplay between inertial stresses within the fluids and dynamic stresses within the interface, and are damped by viscous stresses. During these oscillations, the interface experiences both nonuniform dilatation and shear. By projecting the instant local radius of the interface into the basis of spherical harmonics, the amplitudes of the shape eigenmodes are determined and resonance curves are obtained, allowing the identification of the eigenfrequency ω_n and damping rate β_n of modes of order n from 2 to 4. The knowledge of ω_n and β_n is necessary and sufficient to predict the deformation of a droplet in an unsteady flow. This direct characterization of the interface dynamics makes possible, for fluid systems as complex as crude oil, the prediction of the breakup of a droplet immersed in a turbulent flow, without the need for the exact chemical composition of the fluid system or a description of the interface rheology.

Solving the coupled dynamic equations for the fluids and the interface in the linear regime of oscillation leads to the following conclusions regarding the interface rheology at a high frequency. Two types of interfaces have been considered. Type T1 corresponds to moderately aged interfaces that belong to the first aging regime. Type T2 consists of artificially aged interfaces with a higher coverage rate, which are obtained from a T1 droplet that has been shrunk until the interface displays wrinkles and slightly re-expanded so as wrinkles disappear. In all cases, it is found that the interface rheology is well described by an equivalent two-dimensional isotropic viscoelastic material characterized by dilatational (E_d) and shear (E_s) elasticities, and dilatational (η_d) and shear (η_s) viscosities, which are functions of the frequency ω . A first major result is that the experimental resonance frequencies, which are very large

compared to those of a surfactant-free interface, can only be reproduced by considering shear and dilatation properties of the same order of magnitude: $E_s(\omega) \approx E_d(\omega)$, $\eta_s(\omega) \approx \eta_d(\omega)$. As E_s and η_s are necessarily of an intrinsic nature, we can conclude that intrinsic rheology plays a major role for such interfaces. The question of the contribution of compositional rheology to E_d and η_d remains an open question. However, the fact that E_d and η_d closely behave as E_s and η_s leaves only two options. Either the compositional contribution to E_d and η_d is negligible compared to that of the intrinsic one, or there exists a strong coupling between compositional and intrinsic mechanisms that explains the similitude between E_d and E_s on one side and η_d and η_s on the other side. For a moderately aged interface T1, a second major result is found. The resonant curves obtained at a high frequency are well reproduced by extrapolating the low-frequency power law at higher frequencies. Surprisingly, this indicates that the interface rheology does not change between 0.1 and 80 Hz and therefore that low-frequency tensiometry is relevant throughout this range of frequency. For interfaces T2 that have been artificially aged, the elasticity is significantly larger, which causes a lower value of the ratio between the loss and the conservation moduli. In addition, elasticity is observed to decrease with the frequency in between 80 and 100 Hz, and keeps a constant value between 100 and 130 Hz. This behavior is no longer in agreement with the scaling law observed for a moderately aged interface in the range 0.1–80 Hz. This difference can either be due to a transition of rheological properties at larger frequencies or a change in the structure of the network of adsorbed species at a higher coverage rate. In order to answer this question, future work should explore the dynamics of the T1 interface at higher frequencies and of T2 at lower frequencies. The resonant frequencies of the shape eigenmodes depending on the droplet size, this could be done by changing the droplet volume. However, because of technical limitation of the present setup, this will require building a new apparatus.

In summary, the rheology of a crude oil–water interface over a large range of frequencies is well described by considering an equivalent two-dimensional viscoelastic material, the elasticities and viscosities of which vary as a weak power law of the frequency. This does not imply that there really exists a 2D membrane of constant structure and composition at the interface. First, it means that such a model can be used to predict the deformation of a droplet of diluted crude oil in water. Second, it provides serious constraints on the modeling of physicochemical underlying mechanisms—as the irrelevance of considering a pure compositional interpretation—and hopefully gives some hints for further understanding of the structure of crude oil–water interfaces.

■ APPENDIX I

Transcendental Equation for Eigenmode Determination

Problem Statement. This appendix presents the transcendental equation that is solved to compute the frequencies and the damping rates of the eigenmodes of oscillations of a droplet with a complex interface. This derivation is closely inspired from the seminal works of refs.^{3,12} to which the reader is referred for further details.

We consider a spherical droplet of radius a at equilibrium. The inner and the outer fluids are Newtonian. The density and the viscosity of the inner fluid are respectively ρ_i and η_i , whereas those of the outer fluid are ρ_o and η_o . The interface is modeled as a two-dimensional medium characterized by an equilibrium

interfacial tension γ_e , a Gibbs elasticity E_{Gibbs} , and intrinsic viscoelastic properties: dilatational elasticity E_d , shear elasticity E_s , dilatational surface viscosity η_d , and shear surface viscosity η_s . We consider a surfactant that is soluble in the outer phase and can be adsorbed on the interface. The diffusivity of the surfactant in the bulk fluid is D , whereas its diffusivity on the interface is D_s . Finally, the surface concentration Γ of the surfactant on the interface is considered to be at equilibrium with its volume concentration C in the fluid at the interface. This thermodynamic equilibrium is characterized by the length scale $\Lambda_C = \left(\frac{\partial \Gamma}{\partial C}\right)$. It is worth noting that all these quantities are taken constant and equal to their equilibrium value for a spherical droplet at rest.

The linear oscillations of the droplet at mode n involve 13 physical parameters mentioned above and therefore depend on 10 independent dimensionless groups: the inner Reynolds numbers, $Re_i = \rho_i a^2 \omega_L / \eta_i$ (or the outer one, $Re_o = \rho_o a^2 \omega_L / \eta_o$); the bulk Péclet number, $Pe = a^2 \omega_L / D$; the surface Péclet number, $Pe_s = a^2 \omega_L / D_s$; the density ratio, $\hat{\rho} = \rho_o / \rho_i$; the viscosity ratio, $\hat{\eta} = \eta_o / \eta_i$; the three normalized elasticities, $E_{\text{Gibbs}}^* = E_{\text{Gibbs}} / \gamma_e$, $E_d^* = E_d / \gamma_e$, and $E_s^* = E_s / \gamma_e$; the two normalized surface viscosities, $\eta_d^* = \eta_d / a \eta_i$ and $\eta_s^* = \eta_s / a \eta_i$; the dimensional group that compares the diffusion time scale to the oscillation period, $\lambda = D^{1/2} / \Lambda_C \omega_L^{1/2}$. In these expressions, ω_L is the Lamb frequency, which corresponds to the frequency of oscillation under the assumption of potential flow and pure interface

$$\omega_L^2 = \frac{\gamma_e (n-1)n(n+1)(n+2)}{a^3 (n\rho_o + (n+1)\rho_i)} \quad (8)$$

In spherical coordinates, the location of the droplet interface is defined by its complex local radius \tilde{r} as a function of polar angle θ and the azimuthal angle ϕ . The local radius \tilde{r} is written, for mode (n, m) , as

$$F(\theta, \phi) = \tilde{r} - a(1 + \epsilon_{n,m} Y_{n,m}(\theta, \phi) e^{-\alpha^2 \omega_L t}) = 0 \quad (9)$$

where F is the surface equation, $Y_{n,m}$ are the spherical harmonics, $\epsilon_{n,m}$ is the normalized mode amplitude, and $\alpha^2 = i\omega_n / \omega_L + \beta_n / \omega_L$ is the normalized complex frequency. Modes of the same n but different m are degenerated, which means that they have the same α^2 . For that reason, we will further consider only axisymmetric modes, which correspond to $m = 0$ (i.e., with a normalized amplitude $\epsilon_n = \epsilon_{n,0}$) and which do not depend on the azimuthal coordinate ϕ .

We now present the problem equations, which have been linearized by assuming small amplitude oscillations ($\epsilon_n \ll 1$). In the following, all variables are made dimensionless: lengths are normalized by a , times by ω_L^{-1} , surfactant surface concentrations by Γ_0 , surfactant volume concentrations by Γ_0 / Λ_C (the problem being linear in Γ_0 , we can set $\Gamma_0 = 1$ without loss of generality).

Dynamic Equations for the Fluids. The dynamics of each of the two fluids is driven by the continuity and the Navier–Stokes equations. In the following, subscripts i and o denote the inner and the outer phases, respectively. The continuity equation is

$$\nabla \cdot \mathbf{v} = 0 \quad (10)$$

where \mathbf{v} is the velocity. The linearized Navier–Stokes equation is

$$\frac{\partial \mathbf{v}}{\partial t} = -\nabla p + Re_\chi^{-1} \nabla^2 \mathbf{v} \quad (11)$$

where p is the pressure and the subscript χ stands for either i or o. The solution of these equations is

$$p_i(r) = q_i r^l Y_n(\theta) e^{-\alpha^2 t} \quad (12)$$

$$p_o(r) = q_o r^{-n-1} Y_n(\theta) e^{-\alpha^2 t} \quad (13)$$

$$\mathbf{v} = (v_r \mathbf{e}_r + v_\theta \mathbf{e}_\theta) e^{-\alpha^2 t} \quad (14)$$

$$v_r = \frac{n(n+1)}{r^2} S(r) Y_n(\theta) \quad (15)$$

$$v_\theta = \frac{dS(r)}{dr} \frac{1}{r} \frac{dY_n(\theta)}{d\theta} \quad (16)$$

$$S_i(r) = a_i r j_n(\alpha Re_i^{1/2} r) + \frac{q_i r^{n+1}}{\alpha^2 (n+1)} \quad (17)$$

$$S_o(r) = a_o r h_n^{(1)}(\alpha Re_o^{1/2} r) - \frac{q_o r^{-n}}{\alpha^2 n} \quad (18)$$

where \mathbf{e}_r and \mathbf{e}_θ are the unit vectors; $Y_n = \sqrt{\frac{2n+1}{4\pi}} P_n(\cos \theta)$ is the spherical harmonic of order n , with P_n the Legendre polynomial of order n ; a_i, q_i, a_o, q_o are integration constants that are fixed by the matching conditions at the interface; j_n is the spherical Bessel function of order n , and $h_n^{(1)}$ the spherical Hankel function of the first kind of order n .

Equations for Surfactant Transport. The transport equation of the surfactant concentration through the fluid is

$$\frac{\partial C}{\partial t} = Pe^{-1} \nabla^2 C \quad (19)$$

The transport equation of the surface concentration of surfactant on the interface is

$$\frac{\partial \Gamma}{\partial t} + \nabla_s \cdot (v_\theta \mathbf{e}_\theta)_s + \left(\frac{2v_r}{r} \right)_s = Pe_s^{-1} \nabla_s^2 \Gamma + \lambda Pe^{-1/2} \left(\frac{\partial C}{\partial n} \right)_s \quad (20)$$

where the subscript S denotes that bulk quantities are taken at the interface, and the surface gradient operator can be written as $\nabla_s = \nabla - \mathbf{e}_r (\mathbf{e}_r \cdot \nabla)$.

Matching Conditions at the Interface. The equations for the dynamics of the two fluids and for the surfactant transport are coupled by the matching conditions of the various variables at the interface, which are presented below.

- Kinematic condition that implies that the interface remains in contact with the bulk phases

$$n(n+1) \left[a_i j_n(\alpha Re_i^{1/2}) + \frac{q_i}{\alpha^2 (n+1)} \right] + \alpha^2 \epsilon_n = 0 \quad (21)$$

- Continuity of the radial component of the velocity

$$a_i j_n(\alpha Re_i^{1/2}) + \frac{q_i}{\alpha^2 (n+1)} - a_o h_n^{(1)}(\alpha Re_o^{1/2}) + \frac{q_o}{\alpha^2 n} = 0 \quad (22)$$

- Continuity of the polar component of the velocity

$$a_i [(n-1) j_n(\alpha Re_i^{1/2}) - \alpha Re_i^{1/2} j_{n+1}(\alpha Re_i^{1/2})] + \frac{(n-1) q_i}{(n+1) \alpha^2} - a_o [(n-1) h_n^{(1)}(\alpha Re_o^{1/2}) - \alpha Re_o^{1/2} h_{n+1}^{(1)}(\alpha Re_o^{1/2})] - \frac{(n+2) q_o}{n \alpha^2} = 0 \quad (23)$$

- Stress balance at the interface

$$\mathbf{F}_p + \mathbf{F}_{bv} + \mathbf{F}_{sve} + \mathbf{F}_\gamma = 0$$

\mathbf{F}_p and \mathbf{F}_{bv} are the pressure and bulk viscous stress jumps through the interface. \mathbf{F}_{sve} is the stress generated by surface intrinsic viscosity and elasticity. \mathbf{F}_γ is the stress resulting from dynamic surface tension, which includes equilibrium interfacial tension, Gibbs elasticity, and Marangoni effect.

The normal and polar projections of this equation are written, respectively, as

$$\begin{aligned} & \frac{-Y \epsilon_n}{n(n+1)} + q_i \left[1 - \frac{2n(n-1)}{\alpha^2} \left[\frac{1 - \beta_d}{Re_i} + \frac{YE_{Gibbs}^*}{Gn(n^2-1)(n+2)\alpha^2} \right] \right] \\ & - 2a_i n(n+1) \left[\frac{1 - \beta_d}{Re_i} + \frac{YE_{Gibbs}^*}{Gn(n^2-1)(n+2)\alpha^2} \right] \\ & [(n-1) j_n(\alpha Re_i^{1/2}) - \alpha Re_i^{1/2} j_{n+1}(\alpha Re_i^{1/2})] \\ & - q_o \rho \left[1 - \frac{2(n+1)(n+2)}{\alpha^2 Re_o} \right] + a_o \frac{2\hat{\rho} n(n+1)}{Re_o} \\ & [(n-1) h_n^{(1)}(\alpha Re_o^{1/2}) - \alpha Re_o^{1/2} h_{n+1}^{(1)}(\alpha Re_o^{1/2})] = 0 \end{aligned} \quad (24)$$

$$\begin{aligned} & \frac{q_i}{\alpha^2} \left[2(1-n) + \frac{YE_{Gibbs}^* Re_i}{G(n+1)(n+2)\alpha^2} - n(n-1)\beta_d \right. \\ & \left. - (n-1)(n+2)\beta_s \right] - \frac{2\hat{\eta}(n+2)q_o}{\alpha^2} - a_i \left[2(n^2-1) - \alpha^2 Re_i \right. \\ & \left. - \frac{YE_{Gibbs}^* Re_i}{G(n+2)\alpha^2} + n(n^2-1)\beta_d + (n+2)(n^2-1)\beta_s \right] j_n(\alpha Re_i^{1/2}) \\ & - a_i \left[(2-n(n+1)\beta_d - (n+2)(n-1)\beta_s) \alpha Re_i^{1/2} \right. \\ & \left. + \frac{YE_{Gibbs}^* Re_i^{3/2}}{G(n-1)(n+2)\alpha} \right] j_{n+1}(\alpha Re_i^{1/2}) + a_o \hat{\eta} \\ & [(2(n^2-2) - \alpha^2 Re_o) h_n^{(1)}(\alpha Re_o^{1/2}) + 2\alpha Re_o^{1/2} h_{n+1}^{(1)}(\alpha Re_o^{1/2})] = 0 \end{aligned} \quad (25)$$

where $\mathcal{R} = n\hat{\rho} + n + 1$, $\beta_d = \eta_d^* - \left(\frac{\gamma_e}{\omega_1 \eta_a} \right) \frac{E_d^*}{\alpha^2}$,

$\beta_s = \eta_s^* - \left(\frac{\gamma_e}{\omega_1 \eta_a} \right) \frac{E_s^*}{\alpha^2}$ and

$$G = 1 - \frac{n(n+1)}{\alpha^2 Pe_s} + \frac{n\lambda}{\alpha^2 Pe^{1/2}} - \frac{\lambda H_n(\alpha Pe^{1/2})}{\alpha} \quad (26)$$

with $H_n(\alpha Pe^{1/2}) = h_{n+1}^{(1)}(\alpha Pe^{1/2})/h_n^{(1)}(\alpha Pe^{1/2})$.

It is worth mentioning that, for a low diffusion surfactant ($Pe_s \gg 1$, $Pe \gg 1$), G becomes independent of the Péclet numbers but can still depend on λ .

System to Be Solved. The system of five eqs 21–25 can be recast as a linear system of the form

$$\underline{S}(\alpha) \begin{pmatrix} \epsilon_n \\ a_i \\ q_i \\ a_o \\ q_o \end{pmatrix} = 0 \quad (27)$$

where $\underline{S}(\alpha)$ is a 5×5 matrix. Non-trivial solutions only exist if the determinant of this matrix is zero

$$\det(\underline{S}) = 0 \quad (28)$$

Solving eq 28 leads to the value of α . The frequency ω_n and damping rate β_n of mode n are then obtained as the imaginary and real part of α^2 , respectively.

APPENDIX II

Theoretical Results for Various Modulus Ratios

Additional theoretical results are in Figures 14–16.

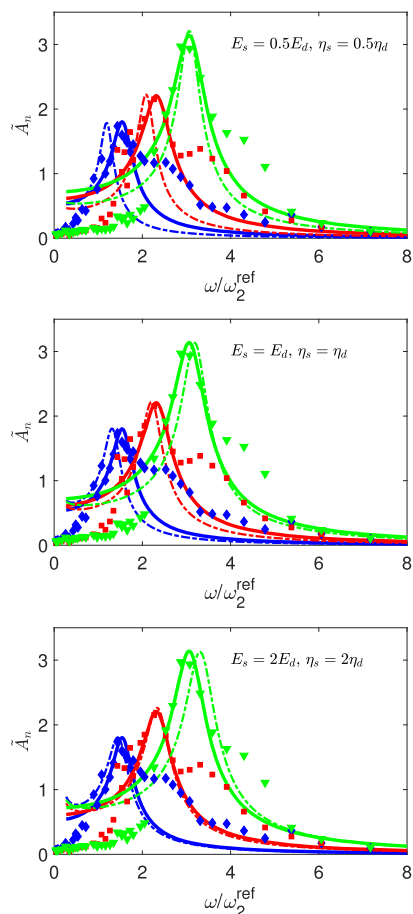


Figure 14. Amplitudes \tilde{A}_n of interface modes 2 (blue), 3 (red), and 4 (green) as a function of the forcing frequency for interface T1. Symbols: measurements. Continuous lines: best fit of each peak by a harmonic oscillator (eq 5). Dashed lines: theory for various ratios E_s/E_d .

AUTHOR INFORMATION

Corresponding Author

*E-mail: frisso@imft.fr.

ORCID

Christine Dalmazzone: 0000-0002-2567-9385

Christine Noik: 0000-0002-5047-252X

Frédéric Risso: 0000-0002-8380-4957

Notes

The authors declare no competing financial interest.

ACKNOWLEDGMENTS

The authors thank Université de Toulouse and Région Occitanie for funding this work.

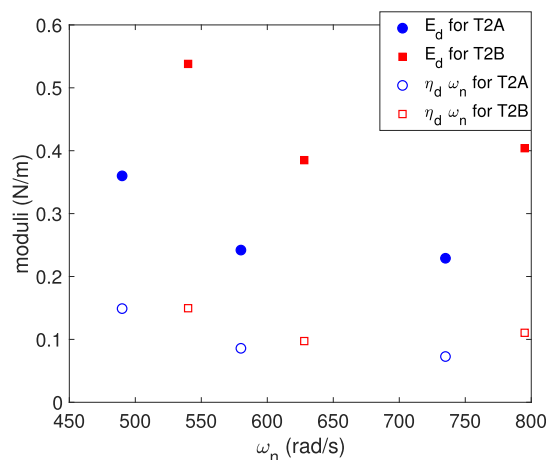


Figure 15. Conservation ($E' = E_d$) and loss ($E'' = \omega_n \eta_d$) moduli determined by matching the frequency and damping predicted by oscillation theory to measured values for interfaces of types T2A and T2B, assuming $E_s = E_d$ and $\eta_s = \eta_d$.

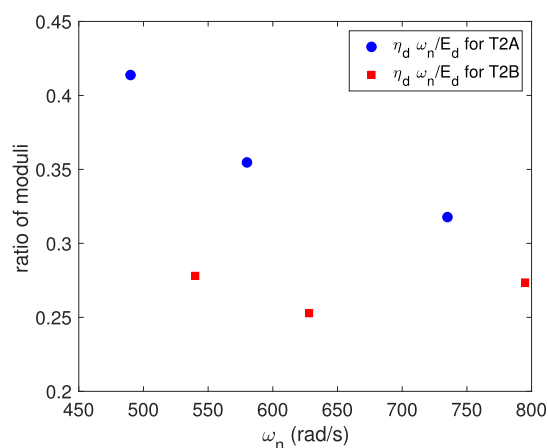


Figure 16. Ratio of loss modulus to conservation modulus from values presented in Figure 15 for interfaces of types T2A and T2B.

REFERENCES

- (1) Hinze, J. O. Fundamentals of the hydrodynamic mechanism of splitting in dispersion processes. *AIChE J.* **1955**, *1*, 289–295.
- (2) Risso, F. The mechanisms of deformation and breakup of drops and bubbles. *Multiphas. Sci. Technol.* **2000**, *12*, 50.
- (3) Miller, C. A.; Scriven, L. E. The oscillations of a fluid droplet immersed in another fluid. *J. Fluid Mech.* **1968**, *32*, 417–435.
- (4) Risso, F.; Fabre, J. Oscillations and breakup of a bubble immersed in a turbulent field. *J. Fluid Mech.* **1998**, *372*, 323–355.
- (5) Galinat, S.; Risso, F.; Masbernat, O.; Guiraud, P. Dynamics of drop breakup in inhomogeneous turbulence at various volume fractions. *J. Fluid Mech.* **2007**, *578*, 85–94.
- (6) Lalanne, B.; Masbernat, O.; Risso, F. A model for drop and bubble breakup frequency based on turbulence spectra. *AIChE J.* **2019**, *65*, 347–359.
- (7) Verwijlen, T.; Imperiali, L.; Vermant, J. Separating viscoelastic and compressibility contributions in pressure-area isotherm measurements. *Adv. Colloid Interface Sci.* **2014**, *206*, 428–436.
- (8) Ivanov, I. B.; Danov, K. D.; Ananthapadmanabhan, K. P.; Lips, A. Interfacial rheology of adsorbed layers with surface reaction: On the origin of the dilatational surface viscosity. *Adv. Colloid Interface Sci.* **2005**, *114–115*, 61–92.
- (9) Prosperetti, A. Normal-mode analysis for the oscillations of a viscous liquid drop in an immiscible liquid. *J. Mec.* **1980**, *19*, 149–182.

- (10) Prosperetti, A. Free oscillations of drops and bubbles: the initial-value problem. *J. Fluid Mech.* **1980**, *100*, 333–347.
- (11) Lu, H.-L.; Apfel, R. E. Quadrupole oscillations of drops for studying interfacial properties. *J. Colloid Interface Sci.* **1990**, *134*, 245.
- (12) Lu, H.-L.; Apfel, R. E. Shape oscillations of drops in the presence of surfactants. *J. Fluid Mech.* **1991**, *222*, 351–368.
- (13) Benjamins, J.; Cagna, A.; Lucassen-Reynders, E. H. Viscoelastic properties of triacylglycerol/water interfaces covered by proteins. *Colloids Surf., A* **1996**, *114*, 245–254.
- (14) Myrvold, R.; Hansen, F. K. Surface Elasticity and Viscosity from Oscillating Bubbles Measured by Automatic Axisymmetric Drop Shape Analysis. *J. Colloid Interface Sci.* **1998**, *207*, 97–105.
- (15) Yu, K.; Yang, J.; Zuo, Y. Y. Droplet Oscillation as an Arbitrary Waveform Generator. *Langmuir* **2018**, *34*, 7042–7047.
- (16) Erni, P.; Fischer, P.; Windhab, E. J.; Kusnezov, V.; Stettin, H.; Lauger, J. Stress- and strain-controlled measurements of interfacial shear viscosity and viscoelasticity at liquid/liquid and gas/liquid interfaces. *Rev. Sci. Instrum.* **2003**, *74*, 4916–4924.
- (17) Soo-Gun, O.-H.; Slattery, J. C. Disk and biconical interfacial viscometers. *J. Colloid Interface Sci.* **1978**, *67*, 516–525.
- (18) Petkov, J. T.; Gurkov, T. D.; Campbell, B. E.; Borwankar, R. P. Dilatational and Shear Elasticity of Gel-like Protein Layers on Air/Water Interface. *Langmuir* **2000**, *16*, 3703–3711.
- (19) Liggieri, L.; Attolini, V.; Ferrari, M.; Ravera, F. Measurement of the Surface Dilational Viscoelasticity of Adsorbed Layers with a Capillary Pressure Tensiometer. *J. Colloid Interface Sci.* **2002**, *255*, 225–235.
- (20) Kotula, A. P.; Anna, S. L. Regular perturbation analysis of small amplitude oscillatory dilatation of an interface in a capillary pressure tensiometer. *J. Rheol.* **2015**, *59*, 85–117.
- (21) Vandebril, S.; Franck, A.; Fuller, G. G.; Moldenaers, P.; Vermant, J. A double wall-ring geometry for interfacial shear rheometry. *Rheol. Acta* **2009**, *49*, 131–144.
- (22) Verwijlen, T.; Moldenaers, P.; Vermant, J. A fixture for interfacial dilatational rheometry using a rotational rheometer. *Eur. Phys. J. Spec. Top.* **2013**, *222*, 83–97.
- (23) Verwijlen, T.; Moldenaers, P.; Stone, H. A.; Vermant, J. Study of the Flow Field in the Magnetic Rod Interfacial Stress Rheometer. *Langmuir* **2011**, *27*, 9345–9358.
- (24) Fruhner, H.; Wantke, K.-D. A new oscillating bubble technique for measuring surface dilational properties. *Colloids Surf., A* **1996**, *114*, 53–59.
- (25) Wantke, K.-D.; Fruhner, H.; Fang, J.; Lunkenheimer, K. Measurements of the surface elasticity in medium frequency range using the oscillating bubble method. *J. Colloid Interface Sci.* **1998**, *208*, 34–48.
- (26) Wantke, K.-D.; Fruhner, H. Determination of Surface Dilational Viscosity Using the Oscillating Bubble Method. *J. Colloid Interface Sci.* **2001**, *237*, 185–199.
- (27) Stadler, D.; Hofmann, M. J.; Motschmann, H.; Shamonin, M. Automated system for measuring the surface dilational modulus of liquid–air interfaces. *Meas. Sci. Technol.* **2016**, *27*, 065301.
- (28) Hofmann, M. J.; Motschmann, H. Surface rheology and its relation to foam stability in solutions of sodium decyl sulfate. *Colloids Surf., A* **2017**, *532*, 472–475.
- (29) Tian, Y.; Holt, R. G.; Apfel, R. E. Investigation of Liquid Surface Rheology of Surfactant Solutions by Droplet Shape Oscillations: Experiments. *J. Colloid Interface Sci.* **1997**, *187*, 1–10.
- (30) Alvarez, G.; Poteau, S.; Argillier, J.-F.; Langevin, D.; Salager, J.-L. Heavy Oil-Water Interfacial Properties and Emulsion Stability: Influence of Dilution. *Energy Fuels* **2009**, *23*, 294–299.
- (31) Sztukowski, D. M.; Yarranton, H. W. Rheology of Asphaltene–Toluene/Water Interfaces. *Langmuir* **2005**, *21*, 11651–11658.
- (32) Bouriat, P.; El Kerri, N.; Graciaa, A.; Lachaise, J. Properties of a Two-Dimensional Asphaltene Network at the Water–Cyclohexane Interface Deduced from Dynamic Tensiometry. *Langmuir* **2004**, *20*, 7459–7464.
- (33) Nenningsland, A. L.; Simon, S.; Sjöblom, J. Influence of Interfacial Rheological Properties on Stability of Asphaltene-Stabilized Emulsions. *J. Dispersion Sci. Technol.* **2014**, *35*, 231–243.
- (34) Samaniuk, J. R.; Hermans, E.; Verwijlen, T.; Pauchard, V.; Vermant, J. Soft-Glassy Rheology of Asphaltenes at Liquid Interfaces. *J. Dispersion Sci. Technol.* **2015**, *36*, 1444–1451.
- (35) Pradilla, D.; Simon, S.; Sjöblom, J.; Samaniuk, J.; Skrzypiec, M.; Vermant, J. Sorption and Interfacial Rheology Study of Model Asphaltene Compounds. *Langmuir* **2016**, *32*, 2900–2911.
- (36) Aske, N.; Orr, R.; Sjöblom, J. Dilatational Elasticity Moduli of Water–Crude Oil Interfaces Using the Oscillating Pendant Drop. *J. Dispersion Sci. Technol.* **2002**, *23*, 809–825.
- (37) Dicharry, C.; Arla, D.; Sinquin, A.; Graciaa, A.; Bouriat, P. Stability of water/crude oil emulsions based on interfacial dilatational rheology. *J. Colloid Interface Sci.* **2006**, *297*, 785–791.
- (38) Pauchard, V.; Sjöblom, J.; Kokal, S.; Bouriat, P.; Dicharry, C.; Müller, H.; al-Hajji, A. Role of Naphthenic Acids in Emulsion Tightness for a Low-Total-Acid-Number (TAN)/High-Asphaltenes Oil †. *Energy Fuels* **2009**, *23*, 1269–1279.
- (39) Quintero, C. G.; Noik, C.; Dalmazzone, C.; Grossiord, J. L. Formation Kinetics and Viscoelastic Properties of Water/Crude Oil Interfacial Films. *Oil Gas Sci. Technol.* **2009**, *64*, 607–616.
- (40) Arla, D.; Flesisnki, L.; Bouriat, P.; Dicharry, C. Influence of Alkaline pH on the Rheology of Water/Acidic Crude Oil Interface. *Energy Fuels* **2011**, *25*, 1118–1126.
- (41) Nguyen, D.; Balsamo, V.; Phan, J. Effect of Diluents and Asphaltenes on Interfacial Properties and Steam-Assisted Gravity Drainage Emulsion Stability: Interfacial Rheology and Wettability. *Energy Fuels* **2013**, *28*, 1641–1651.
- (42) Lucassen, J.; Van den Tempel, M. Dynamic measurements of dilational properties of a liquid interface. *Chem. Eng. Sci.* **1972**, *27*, 1283–1291.
- (43) Winter, H. H.; Chambon, F. Analysis of Linear Viscoelasticity of a Crosslinking Polymer at the Gel Point. *J. Rheol.* **1986**, *30*, 367–382.
- (44) Chambon, F.; Winter, H. H. Linear Viscoelasticity at the Gel Point of a Crosslinking PDMS with Imbalanced Stoichiometry. *J. Rheol.* **1987**, *31*, 683–697.
- (45) Liu, F.; Darjani, S.; Akhmetkhanova, N.; Maldarelli, C.; Banerjee, S.; Pauchard, V. Mixture Effect on the Dilatation Rheology of Asphaltenes-Laden Interfaces. *Langmuir* **2017**, *33*, 1927–1942.
- (46) Bouriat, P. Comment on “Mixture Effect on the Dilatation Rheology of Asphaltenes-Laden Interfaces”. *Langmuir* **2019**, *35*, 2451–2453.
- (47) Sollich, P.; Lequeux, F.; Hebraud, P.; Cates, M. E. Rheology of soft glassy materials. *Phys. Rev. Lett.* **1997**, *78*, 2020–2023.
- (48) Sollich, P. Rheological constitutive equation for a model of soft glassy materials. *Phys. Rev. E: Stat. Phys., Plasmas, Fluids, Relat. Interdiscip. Top.* **1998**, *58*, 738–759.
- (49) Cicuta, P.; Stancik, E. J.; Fuller, G. G. Shearing or Compressing a Soft Glass in 2D: Time-Concentration Superposition. *Phys. Rev. Lett.* **2003**, *90*, 236101.
- (50) Srivastava, S.; Leiske, D.; Basu, J. K.; Fuller, G. G. Interfacial shear rheology of highly confined glassy polymers. *Soft Matter* **2011**, *7*, 1994–1997.
- (51) Van Hooghten, R.; Imperiali, L.; Boeckx, V.; Sharma, R.; Vermant, J. Rough nanoparticles at the oil–water interfaces: their structure, rheology and applications. *Soft Matter* **2013**, *9*, 10791–10798.
- (52) Chebel, N. A.; Risso, F.; Masbernat, O. Inertial modes of a periodically forced buoyant drop attached to a capillary. *Phys. Fluids* **2011**, *23*, 102104.